

NGC 1427A – an LMC type galaxy in the Fornax Cluster

Michael Hilker^{1,2}, Dominik J. Bomans^{3,4}, Leopoldo Infante² & Markus Kissler-Patig^{1,5}

¹ Sternwarte der Universität Bonn, Auf dem Hügel 71, 53121 Bonn, Germany; email: mhilker@astro.uni-bonn.de

² Departamento de Astronomía y Astrofísica, P. Universidad Católica, Casilla 104, Santiago 22, Chile

³ University of Illinois at Urbana-Champaign, 1002 West Green Street, Urbana, IL 61801, USA; email: bomans@astro.uiuc.edu

⁴ Feodor Lynen-Fellow of the Alexander von Humboldt-Gesellschaft

⁵ Lick Observatory, University of California, Santa Cruz, CA 95064, USA

Abstract. We have discovered that the Fornax irregular galaxy NGC 1427A is in very many respects a twin of the Large Magellanic Cloud. Based on B , V , I , and $H\alpha$ images, we find the following. The light of the galaxy is dominated by high surface brightness regions in the south-west that are superimposed by a half-ring of OB associations and H II regions indicating recent star formation. The colors of the main stellar body are $(V - I) = 0.8$ mag and $(B - V) = 0.4$ mag, comparable to the LMC colors. A low surface brightness cloud north of the main body as well as a LSB tail in the west have colors $(V - I \simeq 0.2$ mag) that are more typical for blue compact dwarf galaxies. We identified a system of cluster candidates with mean ages ≤ 2 Gyr (assuming a LMC metallicity) comprising the richest cluster system in an irregular galaxy observed up to now outside the Local Group. In X-ray wavelengths NGC 1427A appears with a relatively soft and complex spectrum.

Key words: Galaxies: individual: NGC 1427A – Galaxies: irregular – Galaxies: photometry – Galaxies: star clusters – X-rays: galaxies

in major axis ($\simeq 2'.4 \times 2'.0$ within the isophote at $\mu_V = 24.7$ mag/arcsec²), slightly larger than the LMC which has a major axis diameter of $\simeq 9.4$ kpc. Table 1 summarizes some properties of NGC 1427A compared with the LMC. The values are from the Third Reference Catalogue of Bright Galaxies (de Vaucouleurs et al. 1991), if no other reference is given.

The projected distance to the central Fornax galaxy NGC 1399 is $22'.9$, about 109 kpc at the cluster distance. Since NGC 1399 has an extended cD halo of about 500 kpc diameter (Schombert 1986, Killeen & Bicknell 1988), one might expect tidal interaction of both galaxies. However, the radial velocities, measured in HI (Bureau et al. 1996), of NGC 1427A ($v_r = 2023 \pm 10$ km s⁻¹) and NGC 1399 ($v_r = 1430 \pm 9$ km s⁻¹) differ by about 600 km s⁻¹ which is nearly twice the cluster velocity dispersion ($\sigma_v = 325$ km s⁻¹, Ferguson & Sandage 1990). NGC 1427A rather agrees with the velocity of NGC 1404 ($v_r = 1944 \pm 15$ km s⁻¹). NGC 1404 is nearly as luminous as NGC 1399 and has a projected distance to NGC 1427A of about 75 kpc.

In this paper we discuss the similarity of the morphological properties of NGC 1427A and the LMC, as well as the stellar content, such as OB associations and young clusters, X-ray properties and the evolutionary state.

The organization of the paper is as follows: In section 2 we describe observation and reduction of the data, section 3 deals with the large scale light distribution of NGC 1427A, section 4 discusses the colors and $H\alpha$ properties of the resolved sources, section 5 discusses the properties of the cluster candidates. Section 6 gives a short discussion of the X-ray informations and in section 7 we summarize our results.

2. Observations and reductions

We obtained long V and I exposures (3×900 s in each color) with the 100' DuPont telescope at Las Campanas Observatory, Chile, in the nights of 26-29 September, 1994. We used a Tektronix 2048 \times 2048 pixel chip, with a

1. Introduction

NGC 1427A is the brightest irregular galaxy in the Fornax cluster. It is about 3 magnitudes brighter than other Fornax galaxies that are classified as irregulars (Ferguson 1989). Its total B magnitude is 13.3 ± 0.21 mag (de Vaucouleurs et al. 1991). Assuming a distance of 16.4 Mpc (Kohle et al. 1996) to the Fornax cluster, the apparent B magnitude corresponds to an absolute magnitude of $M_B = -17.8$ mag, which is nearly identical to the LMC luminosity $M_B = -17.93$ mag, (de Vaucouleurs et al. 1991), assuming a LMC distance modulus of $(m - M) = 18.5$ mag. The linear dimension of NGC 1427A is about 11 kpc

Send offprint requests to: Michael Hilker

Table 1. Some properties of NGC 1427A and of the LMC

Property	NGC 1427A	LMC
distance adopted [kpc]	16400	50.1
B_t^0 [mag]	13.3	0.57
V_t^0 [mag]	12.9	0.13
$(B - V)_0$ [mag]	0.4	0.44
$(V - I)_0$ [mag]	0.8	?
M_B [mag]	-17.8	-17.93
M_V [mag]	-18.2	-18.37
major axis [kpc]	11	9.5
inclination ^{a,b} [°]	48 ± 5	$\simeq 45$
dist. to Milky Way [kpc]		50
proj. dist. to 1399 [kpc]	109	
proj. dist. to 1404 [kpc]	75	
F_{HI} [Jy km sec ⁻¹] ^{a,c}	23.1 ± 1.2	$(1.04 \pm 0.12) \cdot 10^6$
log (HI mass) [M_\odot] ^d	8.79	9.17

^a Bureau et al. 1996 (inclination from face-on)^b Westerlund 1990 (inclination from face-on)^c Huchtmeier et al. 1988^d formula of Roberts 1975

pixel size of $21\mu\text{m}$ or $0''.227$ at the sky, corresponding to a total field of view of $7''.74 \times 7''.74$. The data reduction and calibration is described in Kissler-Patig et al. (1996). The seeing of $0.9''$, measured by the FWHM of stellar images, corresponds to a linear diameter at the Fornax distance of about 72 parsec, which sets our resolution limit (e.g. globular clusters would appear as point sources).

The B exposures (3×1200 s) were obtained with the 40' Swope telescope at Las Campanas Observatory, Chile, in the night of 6/7 December, 1996. We used a SITe #1 2048×2048 pixel chip, with a pixel scale of $0''.694$ at the sky. The seeing was $1.5''$.

The B , V , and I magnitudes of point sources inside NGC 1427A and in its surroundings were derived in the following way: first, we subtracted all objects from the images which were found and fitted with Daophot II (Stetson 1987, 1992). On this cleaned image we replaced all extended objects by values that were interpolated from the surrounding sky or the unresolved stellar component of NGC 1427A. We then smoothed these images by a 7×7 pixel median filter and finally subtracted the results from the original images. The final photometry was done with Daophot II on these images. The colors of all objects were measured on the same images by aperture photometry assuming a constant background of the sky. We used a circular aperture of $2.0''$.

The $\text{H}\alpha$ and R exposures were obtained at Cerro Tololo with the 0.9m telescope in the night of 1/2 December, 1995. We exposed 3×1200 s in $\text{H}\alpha$ and 600 s in R . The seeing was about $1.0''$. The calibration was done by using Landolt (1992) fields.

We retrieved HST WFPC2 images of NGC 1427A in the F606W filter with exposure time of 2×80 s from the STScI data archive. The effective resolution is $0.19''$, or

about 15 pc in Fornax distance. Since the exposure is not deep, we used it only to check for multiplicity of the brightest point sources on the ground-based images where we had overlap.

X-ray observations of NGC 1427A were retrieved from the High Energy Astrophysics Science Archive Research Center (HEASARC) at Goddard Space Flight Center of NASA. The ROSAT PSPC pointing RP600043 is centered on NGC 1399. This pointing also includes NGC 1427A inside the field of view. An X-ray source is clearly present at the position of NGC 1427A. Unfortunately NGC 1427A is located near the window support structure of the telescope, just outside the central $40'$ field of view. Therefore the spatial structure of this source is dominated by the point spread function and the rapid drop of sensitivity to the window support structure.

3. Large-Scale Morphology and Colors of NGC 1427A

The appearance of NGC 1427A resembles that of the LMC with a bar-like main body and several regions of active star formation (Fig. 3). North of the ‘bar’ a large blob of diffuse light and embedded point sources is located, detached from the main body of NGC 1427A (in the following the ‘nob’ = ‘northern blob’). This region appears similar to Shapley Constellation III north of the bar of the LMC.

The appearance at low surface brightness shows that the main body and the ‘nob’ are embedded in a common envelope of unresolved stellar light (see Fig. 4). The lowest isophote in Fig. 4 corresponds to a surface brightness of $\mu_V = 24.7$ mag/arcsec², which is $2\sigma_{\text{sky}}$ above the background. Inside this envelope, the most luminous part of the main body lies off-centered to the south-west. At the south-west border the regions with the highest surface brightness are aligned in a half-ring. The most prominent of these regions is located at (530,360) in (X,Y) pixel coordinates of Fig. 4. Appearance and size (~ 1.3 kpc) of this star forming region strongly resembles the 30 Dor complex in the LMC. The east side of the ‘bar’ ends in an extended tail of low surface brightness ($\mu_V \simeq 23.0$ mag/arcsec²). At the southern border of the ‘nob’ some low surface brightness spurs point towards the main body of the galaxy (see Fig. 4).

Fig. 1. This picture shows a $(V - I)$ color map of NGC 1427A. The greyscale corresponds to color bins of 0.1 mag as indicated in the plot. The sky is arbitrarily set to a color of $(V - I) = 1.1$ mag. Arrows indicate the direction to the central Fornax galaxies NGC 1399 and NGC 1404.

We constructed a calibrated color map from our V and I image to visualize the colors of the main body and the bright knots (Fig. 1). All pixels with intensities lower

than 2σ above the sky were arbitrarily set to $(V - I) = 1.1$ mag. The color map was smoothed by a 7×7 pixel median filter and the color values were binned in steps of 0.1 mag. The mean color error is in the order of 0.03 mag in the region of the stellar body. Several features become visible: the bright knots have colors bluer than $(V - I) = 0.65$ mag. The stellar body has a mean color of $(V - I) = 0.8 \pm 0.03$ mag except a north-south stripe in the middle of the galaxy with colors around $(V - I) = 0.9 \pm 0.03$ mag. This redder color is probably due to a dust lane at the center of the galaxy. Another explanation would be an older (redder) stellar population that is dominating the color in this region. The ‘nob’ as well as the faint luminosity tail in the east have significantly bluer colors of about $(V - I) = 0.7 \pm 0.04$ mag, which indicates a different star formation history in these regions than in the main body.

We also measured $(B - V)$ colors of the stellar body in small apertures assuming constant sky values. The mean colors are $(B - V) = 0.4 \pm 0.04$ mag in the main body, which is comparable to the mean color of the LMC, $(B - V) = 0.3 \pm 0.04$ mag in the eastern tail, and $(B - V) = 0.2 \pm 0.04$ mag in the ‘nob’. Compared to other galaxies the ‘nob’ lies in the color range of blue compact dwarf galaxies (hereafter BCDs) or very blue dwarf irregular galaxies (i.e. Thuan 1983, Gallagher & Hunter 1987).

The blue color of the unresolved stellar light can not be explained by an old stellar population alone, even if this population would have a very low metallicity of $Z = 0.001$. Therefore a young stellar component must have contributed to the light. We estimated ages by comparison with photometric evolutionary synthesis models of dI and BCD galaxies from Krüger & Fritze-v. Alvensleben (1993). In the case of continuous star formation a color of $(B - V) = 0.4$ of the main body is consistent with ages between 2 and 5 Gyr depending on metallicity and a constant or decreasing star formation rate (SFR). The stellar population of the ‘nob’ with $(B - V) = 0.2$ would then be about 1 Gyr old. Assuming a single starburst occurring in a 10 Gyr old galaxy with a previous continuous SFR, colors bluer than $(B - V) = 0.4$ correspond to ages younger than 10^8 yr after the burst.

4. Extended Objects and H α distribution

The luminosities of point sources and slightly extended objects in and around NGC 1427A were determined by PSF fitting in the B , V , and I images. The colors were measured in apertures of $2.0''$ diameter assuming constant sky values. We present in the following foremost results using the $(V - I)$ colors, because the resolution in the B image is not as good as in the V and I images due to the larger pixel scale and the worse seeing. About 30% of the objects we found in V and I could not be measured in B . Figure 2 shows in the upper panel the color magnitude diagram (CMD) of all objects within a radius of about 8

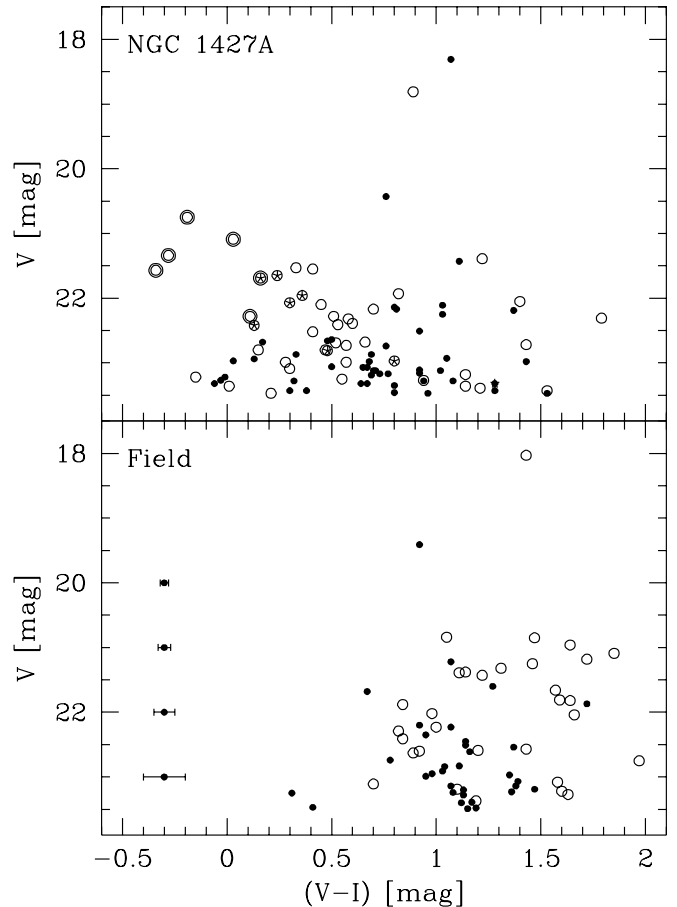


Fig. 2. The top panel shows a CMD of all objects within a radius of $1.7'$ from the center of NGC 1427A. The dots are unresolved objects as discussed in section 5. Circles indicate slightly extended objects (the FWHM is more than 1.5 times larger than for stellar images). Circles with stars inside are objects with H α emission. Double circles turned out being multiple objects after comparison with the HST image. The lower panel shows the CMD of objects in a 2 times larger control field north of NGC 1427A. The mean errorbars of the color for different magnitudes are indicated.

kpc ($\approx 1.7'$) from the geometrical center of NGC 1427A (which is the center of the faintest isophote). In the lower panel the CMD for a two times larger control field located $5'$ north of NGC 1427A is plotted. Objects redder than $(V - I) = 0.8$ mag in both panels most probably are resolved as well as unresolved background galaxies and foreground stars. The slight excess of extended objects in the control field compared to the target field can be explained by statistical fluctuations. Comparison of the two CMDs shows clearly that NGC 1427A sample is dominated by very blue objects.

Figure 3 shows the V image of NGC 1427A with H α contours overplotted. Our H α image is not deep enough to search for diffuse filaments and shells similar the supergiant shell around Shapley Constellation III in the LMC

Fig. 3. This picture shows a V image of NGC 1427A. The white contours indicate H α detections. The values are aperture ($V - I$) and ($B - V$) colors for the brightest, most prominent OB associations and clusters. In comparison to Fig. 4 the (X,Y) pixel section of this image is (320,190) for the lower left corner and (830,700) for the upper right corner.

Fig. 4. The location of the cluster candidates is given in the plot of the isophotes of the main stellar body of NGC 1427A. The distribution of the clusters is more uniform than that of the OB associations (see also Fig. 3). The contours are derived from a 10×10 pixel median filtered image. The 3 lowest isophotes correspond to $\mu_V = 24.7$ mag/arcsec², $\mu_V = 24.1$ mag/arcsec², and $\mu_V = 23.6$ mag/arcsec², respectively. Frame size and orientation are the same as in Fig. 1.

(e.g. Meaburn 1980, Kennicutt et al. 1995). The aperture ($V - I$) and ($B - V$) colors of the most prominent blue knots are indicated. Almost all regions that are associated with H α emission show very blue components with colors in the range $-0.3 < (V - I) < 0.4$ mag (or $-0.1 < (B - V) < 0.2$ mag). In some cases the ($V - I$) color is negative, whereas the ($B - V$) color is positive. This can only be explained by the strong contribution of emission lines in the V filter. The most prominent emission lines of H II regions in the V band are the O III lines at 4959 and 5007 Å. A comparison with the HST image shows that most of the bright blue knots are multiple objects. Thus, from their color and sizes these objects can be regarded as OB associations and H II regions.

5. Properties of Cluster Candidates

We defined as cluster candidates those objects that are clearly unresolved in our V image, i.e. those objects that have FWHM of the PSF smaller than $1.2''$ (see the dots in Fig. 2). The HST image shows that most of these objects are also unresolved at its higher resolution, as one would expect, since even the largest Milky Way globular clusters would appear hardly resolved at Fornax distance. (Note that the fainter clusters and objects in the planetary camera image could not be measured due to the short exposure time of the HST image). We counted all objects within $80''$ radius from the geometrical center within the lowest isophotes. These objects are uniformly distributed over the whole area, contrary to the light of the main stellar body and the OB association (see Fig. 4).

Applying the same selection criteria as for the NGC 1427A cluster candidates we counted objects in a background control field $5'$ north of NGC 1427A. We subtracted the area corrected background counts from the galaxy object counts in color bins of 0.15 mag as well as in magnitude bins of 0.5 mag. Figures 5, 6 (upper panels), and 7 show the resulting histograms. The color histograms are selected for objects brighter than $V = 23.5$ mag. As men-

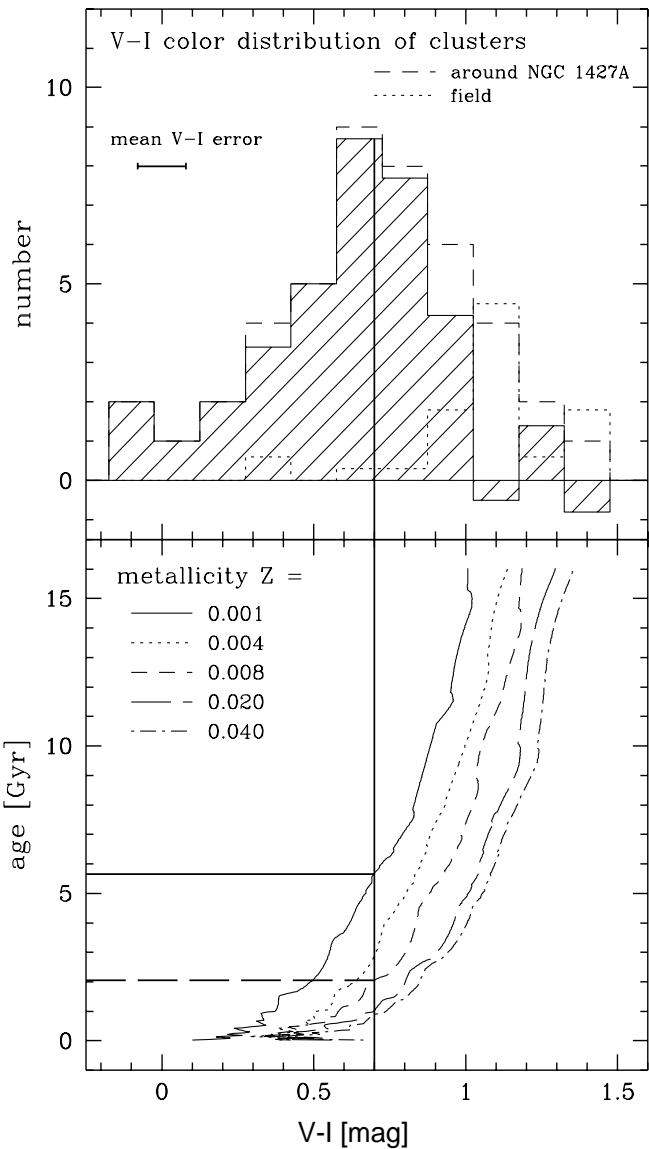


Fig. 5. The hashed histogram (upper panel) shows the ($V - I$) color distribution of clusters in NGC 1427A after a statistical subtraction of background objects (dotted histogram). The mean error is indicated. Note that the colors of the bluest clusters are contaminated by emission lines of nearby H II regions. The lower panel illustrates the color evolution of clusters as function of metallicity according to Fritze v. Alvensleben & Kurth (1997). The peak color ($V - I$) = 0.7 mag corresponds to an age of about 2.0 Gyr assuming an LMC metallicity.

tioned above not all objects could be measured in the B image. Thus, the ($B - V$) color distribution only contains about 80% of the objects of the ($V - I$) color distribution.

The ($V - I$) color histogram shows a main concentration of objects around ($V - I$) = 0.7 mag with a tail to bluer colors and a few objects with ($V - I$) \simeq 0.9 mag. Colors bluer than ($V - I$) = 0.8 mag can not be explained by a low metallicity alone, since even the metal poorest clusters in our Milky Way have redder ($V - I$) col-

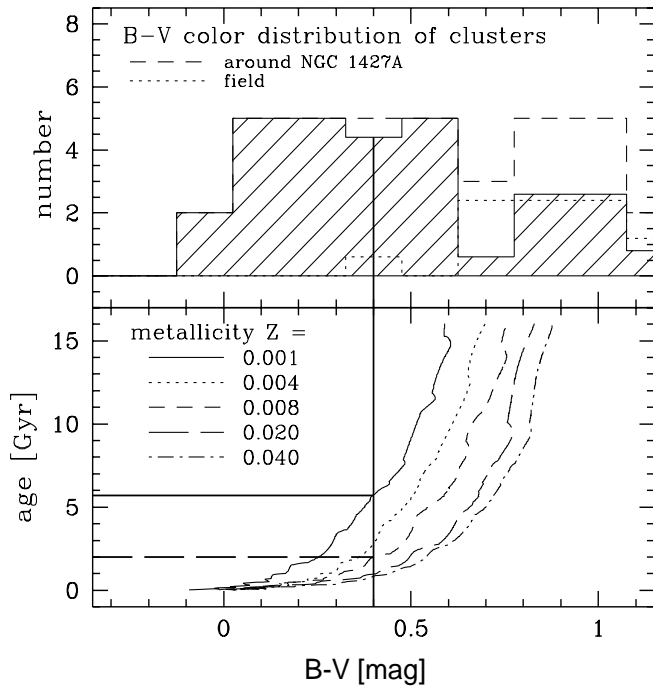


Fig. 6. The hashed histogram shows the $(B - V)$ color distribution of clusters in NGC 1427A after a statistical subtraction of background objects (dotted histogram). As in Figure 5 the lower panel illustrates the comparison to color evolution models of clusters.

ors (e.g. Mc Master catalogue, Harris 1996). Concerning the $(B - V)$ color most cluster candidates are distributed between $0.0 < (B - V) < 0.6$ mag. The mean photometric errors are $\sigma_{(V-I)} = 0.08$ mag and $\sigma_{(B-V)} = 0.10$ mag.

We can estimate age limits for the objects in dependence of metallicity. To do so, we used the models of Fritze v. Alvensleben & Kurth (1997, private communication, update of Fritze v. Alvensleben & Burkert 1995). The lower panels in Figure 5 and 6 illustrate the dependence between color, age and metallicity for a stellar population that experienced a single star burst like star clusters. In the metal poorest ($Z = 0.001$) models, the bulk of the clusters with $(V - I) < 0.8$ mag (or $(B - V) < 0.5$ mag) would be younger than 7 Gyr. Only the clusters at $(V - I) = 1.0$ mag (or $(B - V) = 0.6$ mag) could represent old metal poor globular clusters. Assuming a LMC metallicity ($Z = 0.008$), the reddest clusters ($(V - I) = 0.9$ mag) would have ages of about 5 Gyr, whereas the peak color $(V - I) = 0.7$ mag would be consistent with an age of 2 ± 1 Gyr. This age is also consistent with the results in the $(B - V)$ color (see Fig. 6). In this case, the colors as well as the ages of the NGC 1427A clusters are comparable to (but perhaps slightly redder/older than) the intermediate age clusters in the LMC (Arimoto & Bica 1989).

The luminosity function of the cluster candidates appears to be complete down to $V \simeq 23$ mag which corresponds to an absolute magnitude of $M_V \simeq -8$ mag. The

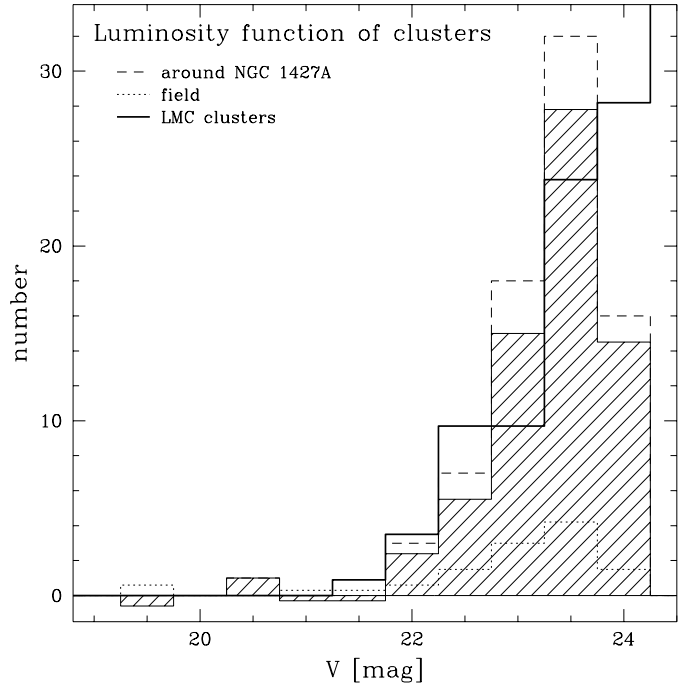


Fig. 7. The hashed histogram shows the V luminosity function of clusters in NGC 1427A after a statistical subtraction of background objects (dotted histogram) from the raw counts (dashed histogram). The brightest objects have absolute magnitudes of about $M_V = -9.0$ mag comparable to the luminosity of the brightest LMC clusters. The thick line represents the counts of the star clusters in the LMC (Bica et al. 1996) corrected for the Fornax distance and normalized to the luminosity of NGC 1427A.

brightest objects have absolute magnitudes of the order of the brightest LMC clusters, as for example NGC 1850 ($M_V = -9$ mag, Bica et al. 1996). The number of clusters in NGC 1427A down to $M_V = -8$ mag is about 0.75 times the cluster counts in the LMC (see Table 2). Normalized to the absolute luminosity of their host galaxies, the counts are comparable. Figure 7 shows the luminosity function of the NGC 1427A clusters in comparison to the one of the LMC clusters after correction for the Fornax distance and normalization to the luminosity of NGC 1427A. The LMC cluster counts are based on the list of Bica et al. (1996). We included only objects that are classified as “star cluster”. Our analysis shows that NGC 1427A has the richest system observed in an irregular galaxy more distant than the Magellanic Clouds up to now. The old cluster population of the LMC has colors of about $(V - I) = 1.0$ mag and absolute magnitudes $M_V > -8.5$ mag, which is close to

Table 2. Cluster counts in NGC 1427A and the LMC

	$M_V < -9.0$	$M_V < -8.5$	$M_V < -8.0$
1427A	0	4	15
LMC	1	11	20

our completeness limit. The distribution of the old LMC clusters is very extended around the LMC, which implies that we will miss corresponding objects in NGC 1427A as a consequence of our statistical background correction. Both effects result in a bias against the detection of true old clusters in our data.

6. X-ray properties

NGC 1427A is clearly detected with ROSAT PSPC (observation RP600043) as an X-ray source with 445 ± 36 net photons in the full spectral range of the ROSAT PSPC (0.1 to 2.4 keV). The spectrum appears to be relatively soft with most of the photons at energies lower than 1 keV. Neither a fit with a Raymond-Smith thin plasma, nor a power law gave an acceptably good fit to the spectrum. This may imply that the spectrum is a composite of emission from stars, supernovae, and true diffuse hot gas, typical for an irregular galaxy (see e.g. Bomans et al. 1997). We can estimate a total luminosity in the 0.5–2.0 keV band of the ROSAT PSPC to be 5×10^{39} ergs s⁻¹, adopting our distance modulus and a foreground absorption of 6×10^{20} cm⁻². This appears somewhat higher than the only published X-ray luminosity of the LMC (Wang et al. 1991), but both the Einstein IPC data of the LMC and the unsatisfactory fit to our ROSAT PSPC spectrum of NGC 1427A leave a significant margin of uncertainty. We conclude, that both the X-ray luminosity and hardness of NGC 1427A are not atypical for a large irregular galaxy (Bomans et al. 1997) and similar to the values of the LMC. Much deeper and higher spatial and spectral resolution data (with the upcoming X-ray satellites AXAF and XMM) are necessary to investigate the origin of the X-ray emission of NGC 1427A further. Also an integrated spectrum and a total X-ray luminosity of the LMC derived from the ROSAT All Sky Survey would be of great value for future studies of the X-ray properties of more distant star forming galaxies.

7. Summary

The irregular galaxy NGC 1427A is comparable in size, luminosity and color to the LMC. The brightest stellar populations of the galaxy are offset to the south-west compared to its nearly elliptical/disk shape at low isophotes. At the south-west border we identified a half-ring of OB associations and H II regions, which indicate recent star formation. The colors of the ‘nob’ and the low surface brightness tail in the east are consistent with starburst ages less than some 10^8 years, showing a different star formation history than the main body of NGC 1427A. We found about 34 cluster-type objects down to $V = 23.5$ mag that are uniformly distributed over the galaxy. Their color as well as their luminosity distribution is comparable to the intermediate age cluster population of the LMC. Assuming a LMC metallicity the clusters have mean ages less

than 2 Gyr, except a few clusters that might be genuine old globular clusters. In the X-ray NGC 1427A appears similar to the LMC with a relatively soft and complex spectrum and a luminosity in the order of 10^{40} ergs s⁻¹.

NGC 1427A appears to be nearly a twin of the LMC in all the investigated properties. It is interesting to note, that NGC 1427A shows also some signs for tidal influence on the star formation history. The ages of clusters point at a dominating cluster formation event a few Gyr ago, which accounts for most of the cluster candidates in our data. A sudden event of cluster formation 2 Gyrs ago is well known in the LMC (e.g. Bomans et al. 1995, Girardi et al. 1995) and is thought to be triggered by interaction with the Milky Way. There are several conceivable scenarios that might be responsible for the present appearance of NGC 1427A. Cellone & Forte (1997) interpreted the ‘nob’ as a separate dwarf galaxy and concluded that the particular appearance of NGC 1427A is due to the collision between two galaxies. A similar scenario was suggested by Freeman & de Vaucouleur (1974) for the folded ring galaxy Arp 144. According to this view the distorted appearance and the elongated ring of this galaxy may be due to the encounter with an intergalactic gas cloud, and possibly triggering starbirth regions both in the galaxy and the remainder of the cloud. In our case the former cloud candidate could be the ‘nob’. Nevertheless, the fact that the ‘nob’ and the main body of the galaxy are embedded in common and rather symmetrical envelope may support our interpretation of the ‘nob’ being an original part of NGC 1427A.

Alternatively, one may speculate about the passage of NGC 1427A through the gas associated with the Fornax cluster as trigger for the subsequent star formation. If this is the case, the main starburst event must have appeared as the galaxy started crossing the dense region in the cluster core near NGC 1399 or NGC 1404. As judged from the cluster candidates in NGC 1427A, this must have happened about 2 Gyr ago. The question, which of these scenarios should be preferred and whether the ‘nob’ represents an initially distinct object or belongs to NGC 1427A, can only be solved by dynamical analysis from high resolution HI measurements and optical spectra.

Acknowledgements. We thank our referee Dr. B.E. Westerlund for helpful comments. Our paper was partly based on observations made with the NASA/ESA Hubble Space Telescope, obtained from the data archive at the Space Telescope Science Institute. STScI is operated by the Association of Universities for Research in Astronomy, Inc. under the NASA contract NAS 5-26555. This research was supported by the DFG through the Graduiertenkolleg ‘The Magellanic System and other dwarf galaxies’ and under grant Ri 418/5-1. DJB acknowledge partial support by the Alexander von Humboldt-Gesellschaft and thanks S. Points for service observations at the CTIO 0.9m telescope. LI wish to thank FONDECYT (grant # 8970009) and a 1995 Presidential Chair in Science for partial support.

References

- Arimoto N., Bica E., 1989, A&A 222, 89
- Bica E., Clariá J.J., Dottori H., Santos J.F.C., Piatti A.E., 1996, ApJS 102, 57
- Bomans, D.J., Chu, Y.-H., Hopp, U. 1997, AJ 113, 1678
- Bomans, D.J., Vallenari A., de Boer K.S., 1995, A&A 298, 427
- Bureau M., Mould J.R., Staveley-Smith L., 1996, ApJ 463, 60
- Cellone S.A., Forte J.C., 1997, AJ 113, 1239
- Ferguson H.C., 1989, AJ 98, 367
- Ferguson H.C., Sandage A., 1990, AJ 100, 1
- Freeman K.C., de Vaucouleur G., 1974, ApJ 194, 569
- Fritze-v. Alvensleben U., Burkert A., 1995, A&A 300, 58
- Fritze-v. Alvensleben U., Kurth O., 1997, private communication
- Gallagher J.S., Hunter D.A., 1987, AJ 94, 43
- Girardi L., Chiosi C., Bertelli G., Bressan A., 1995, A&A 298, 87
- Harris W.E., 1996, AJ 112, 1487
- Huchtmeier W.K., Richter O.-G., 1988, A&A 203, 237
- Kennicutt R.C., Bresolin F., Bomans D.J., Bothun G.D., Thompson I.B., 1995, AJ 109, 594
- Killeen N.E.B., Bicknell G.V., 1988, ApJ 325, 165
- Kissler-Patig M., Kohle S., Hilker M., Richtler T., Infante L., Quintana H., 1996, A&A 319, 470
- Kohle S., Kissler-Patig M., Hilker M., Richtler T., Infante L., Quintana H., 1996, A&A 309, L39
- Krüger H., Fritze-v. Alvensleben U., A&A 284, 793
- Meaburn J., 1980, MNRAS 192, 365
- Roberts M.S., 1975, in "Galaxies and the Universe", eds. A. Sandage, M. Sandage, and J. Kristian, University of Chicago Press, Chicago, p. 309
- Schombert J.M., 1986, ApJS 60, 603
- Stetson P.B., 1987, PASP 99, 191
- Stetson P.B., 1992, in: "Astronomical Data Analysis Software and Systems I, A.S.P. Conference Series, Vol. 25, eds. D.M. Worrall, C. Biemesderfer, and J. Barnes, p. 297
- Taylor C.L., Brinks E., Pogge R.W., Skillman, E.D., 1994, AJ 107, 971
- Thuan T.X., 1983, ApJ 268, 667
- Vaucouleurs de G., Vaucouleurs de A., Corwin H.G., Buta R.J., Paturel G., Fouqué P., 1991, Third Ref. Catalogue of Bright
- Westerlund B.E., 1990, A&AR 2, 29

This figure "fig1.gif" is available in "gif" format from:

<http://arXiv.org/ps/astro-ph/9707151v1>

This figure "fig3.gif" is available in "gif" format from:

<http://arXiv.org/ps/astro-ph/9707151v1>

This figure "fig4.gif" is available in "gif" format from:

<http://arXiv.org/ps/astro-ph/9707151v1>